



## Utilization of Cross-linked Chitosan/ ACTF Biocomposite for Softening Hard Water: Optimization by Adsorption Modeling



R. Hosny<sup>1\*</sup>, M. Fathy<sup>2</sup>, Omnia H. Abdelraheem<sup>3</sup> and M.A. Zayed<sup>4#</sup>

<sup>1</sup>Production Department, Egyptian Petroleum Research Institute (EPRI), 1 Ahmed El-Zomer, Nasr City, Box. No. 11727, Cairo, Egypt

<sup>2</sup>Petroleum Applications Department, Egyptian Petroleum Research Institute (EPRI), 1 Ahmed El-Zomer, Nasr City, Box. No. 11727, Cairo, Egypt

<sup>3</sup>Engineering Sciences Department, Faculty of Engineering, Beni-Suef University, Beni-Suef, Egypt

<sup>4</sup>Chemistry Department, Faculty of Science, Cairo University, Giza 12613, Egypt.

In this study cross-linked biocomposite with a high adsorption capacity was prepared by incorporating amorphous carbon thin film (ACTF); synthesized from rice straw by catalytic acid spray method; into the chitosan biopolymeric matrix by microwave irradiation precipitation technique. The new technique improves the polymeric cross-linking effect between ACTF and chitosan without catalyst and does not affect the spatial structure of chitosan. The physicochemical properties of the resulting biocomposite were evaluated by FTIR, SEM, XRD, Raman. The chitosan/ACTF biocomposite analyses refer to the presence of cave-shaped pores, high electron density and ion exchange active sites on internal and external surfaces in addition to high thermal stability. The adsorption study summarizes the potential of novel chitosan/ACTF biocomposite for the removal of  $\text{Ca}^{2+}$  and  $\text{Ba}^{2+}$  from water by batch adsorption. Freundlich isotherm model was best fitted to equilibrium data as well as the pseudo-second-order kinetic model was best fitted to adsorption kinetic data. Thermodynamic parameters ( $\Delta G$ ,  $\Delta H$ , and  $\Delta S$ ) suggested the exothermic nature of  $\text{Ca}^{2+}$  and  $\text{Ba}^{2+}$  adsorption. The removal efficiency for  $\text{Ca}^{2+}$  and  $\text{Ba}^{2+}$  were 80% and 87.85 % at initial concentration of 100 mg/l, respectively. The results indicated that the chitosan/ACTF biocomposite has a high adsorption capacity and excellent water compatibility.

**Keywords:** Chitosan/ACTF biocomposite; Microwave; Water treatment; Water softening, Adsorption of  $\text{Ca}^{2+}$  and  $\text{Ba}^{2+}$  ions; Adsorption models; Adsorption kinetic.

### Introduction

Water management, particularly in developing countries, highlights the momentum needed to focus on the present challenges. Access to safe drinking water is growing as a life and development issue at the national, regional and universal levels [1,2]. There are many commercial ways of hard water treatment including water softeners, reverse osmosis and water filters. Adsorption system is one of the most common water treatment systems [3].

Cahyaningrum [4] studied the removal of  $\text{Mg}^{2+}$  ion from water in a batch adsorption system by chitosan beads. Kano [5] conducted adsorption

experiment from aqueous solutions containing known amount of Cr (chromium) using chitosan was explored to evaluate the effect of common ions  $\text{Na}^+$ ,  $\text{K}^+$ ,  $\text{Mg}^{2+}$ ,  $\text{Ca}^{2+}$  for  $\text{Cr}^{3+}$ , and  $\text{Cl}^-$ ,  $\text{NO}_3^-$ ,  $\text{SO}_4^{2-}$  for  $\text{Cr}^{+4}$  on the efficiency of chitosan as sorbent for Cr. Fathy [6] synthesized sulfonated ion Exchange polystyrene biocomposite resin for  $\text{Ca}^{2+}$  hardness removal. Mahatmanti [7] applied chitosan-based membrane mixed with rice hull ash (RHA) silica and polyethylene glycol (PEG) as adsorbent of  $\text{Ca}^{2+}$ ,  $\text{Mg}^{2+}$ ,  $\text{Zn}^{2+}$  and  $\text{Cd}^{3+}$  in an aqueous solution. Magnetic nanoparticles /chitosan had been adopted in the field of adsorption/ biosorption for separation of pollutants from aqueous solutions by Mohseni-Bandpi [8].

\*Corresponding author e-mail: dr.rashahosny@yahoo.com

#E-mail: mazayed429@yahoo.com, Tel: 002-02-22728437, 002-01005776675, Fax: 002-02-35728843.

Received 07/05/2019; Accepted 01/10/2019

DOI: 10.21608/ejchem.2019.12589.1780

©2019 National Information and Documentation Center (NIDOC)

Amorphous carbon thin films (ACTF) is a novel form of permeable carbon materials for different applications such as absorbent in vapor and liquid phases [9&10]. In general, the synthetic fabrication of these materials are relatively complex, time-consuming, and entails higher costs. A novel simple low-cost method was developed by [11]. The researchers synthesized ACTF from rice straw and investigated its structure and characteristics as new adsorbents of  $\text{Na}^+$  from synthetic water. Also, Fathy [12] synthesized ACTF from oil palm leaves. According to El-Sayed [13] amorphous carbon thin films ACTF was synthesized from sawdust used effectively to remove oil from water with high adsorption capacity [14].

Biomass microwave irradiation is a promising treatment process because it uses thermal and (non-thermal) effects. Therefore, microwave irradiation has been widely used in all fields of synthetic chemistry such as polymer synthesis [15].

In order to fully utilize the amorphous thin-film carbon (ACTF) and chitosan as adsorbents, this work is designed to fabricate and characterize a novel biocomposite of chitosan / ACTF, by applying the microwave in a single-phase method. By Comparing with the methods described in the literature, the methodology in this work is simpler and produces a high yield of the mass production with low-cost. The study then explored the optimization and modeling of calcium and barium cations adsorption by chitosan / ACTF bi-polymer, which was synthesized as an effective adsorbent to remove hardness in groundwater.

## **2. Experimental**

### *ACTF*

Amorphous carbon thin film ACTF prepared from waste rice straw according to a novel technique developed by Fathy, et al. [11] including the rice straw treatment to produce cellulose mass that was enclosed to a reaction with prepared cobalt silicate nanoparticle as a catalyst and chemical exfoliation of cellulose. The same method was applied in our previous works to prepare ACTF from different precursors: sawdust, and oil palm leaves [13 & 15]. Physicochemical properties and microstructure of ACTF were investigated using Raman spectrometer, thermogravimetry analyzer, transmission electron microscope, scanning electron microscope [12].

ACTF actually has a unique multilayered sandwich-like structure composed of oxidized graphene and activated carbon layers, with a large specific surface area. Furthermore, the investigation proved that prepared ACTF molecules having both hydrophilic (polar) and hydrophobic (nonpolar) properties, so ACTF shows high ability to disperse in both polar and non-polar solvents [16]. The percentage yield of the rice straw-based ACTF prepared according the following is to 79.41 % yield of the precursor (cellulose mass), and to our knowledge, it should be the highest value reported for ACTF in similar experimental conditions by now.

The method goes through four phases. Firstly the rice straw with hot distilled water dried overnight at 60°C, grinded to sizes (0.7–0.1 mm) and stored in a tight bottle until used. The second phase is the chemical exfoliation of cellulose. Hence, the dried precursor was hydrolyzed for 60 min at 120°C, using 1% (wt/wt) sulphuric acid. An amount of 5 g of precursor was added in the presence of 0.1 g silica to 5 ml concentrated sulfuric acid (The acid added by spraying while keeping stirring for 10 min), filtrated and washed with hot deionized water till pH 7. The following phase is drying at 40°C for 6 h. Finally, the carbonization process is accomplished, where the semi carbonized sample mixed with 0.01 g prepared cobalt silicate nanoparticle [17], heated up to 40°C for 30 min. Finally, the prepared amorphous carbon thin film (ACTF) left to cool for 1 h, then dried in a vacuum oven for 24 h at 50°-70°C [11].

For Chitosan/ACTF biocomposite preparation purpose, a suspension of ACTF is prepared by mixing 0.05 g of ACTF in 250 ml distilled water, then sonicated for 10 min using ultrasonic. No surfactant is needed, due to the unique properties of the synthesized amorphous carbon with a significant affinity for dispersion in water.

### *Chitosan modification*

Chitosan/ distilled water suspension (3% w/v) was prepared. In order to dissolve Chitosan, 25 ml of 1.0 M HCl was added dropwise with stirring. The pH was adjusted to 5.3 by using 1.0 M NaOH. Subsequently. In a domestic modified microwave oven (700W, Midea EG7KCW3-NA, China), 20 ml of the produced solution was heated to (45°C) for 1 min radiation time and then cooled to room temperature [18].

#### *Chitosan/ACTF biocomposite preparation*

The Chitosan/ACTF biocomposite was prepared by a microwave precipitation method based on a new developed single-stage method under microwave radiation without the addition of activation agent (catalysis synthesis process); i.e., no post-treatment stage is required.

The chitosan/ACTF biocomposite was obtained by slow injection of the prepared suspension of ACTF (50 ml) injection volume at a flow rate of 15 ml/min using a 21-gauge syringe needle with keeping stirring at 400 rpm in the microwave for 30 min. The produced suspension then centrifuged at 100 rpm for 20 min to remove the deposit. The deposited Chitosan/ACTF beads were immersed in 1% (v/v) of HCl aqueous solution overnight in order to induce and stabilize crosslinking effect [19]. Finally, the obtained Chitosan/ACTF beads were dried at 60 °C for 6 h and washed with successive doses of 500 ml hot water.

#### *Solutions*

Synthetic stock solutions were prepared by dissolving Ca<sup>+2</sup> and Ba<sup>+2</sup> in forms of CaCl<sub>2</sub>·2H<sub>2</sub>O and BaCl<sub>2</sub>·4H<sub>2</sub>O salts in distilled water. Series of diluted concentrations were prepared. The resultant solutions from adsorption testes were centrifuged at 4000 rpm for a while and supernatants were subjected to quantitative analysis. The concentrations of Ca<sup>+2</sup> were measured by atomic absorption spectroscopy (ZEEnit 700, from Analytik Jena), where barium concentrations were followed up by Ion chromatography (Dionex Ion chromatography (IC) DX 600 system).

#### *Chitosan and ACTF/Chitosan biocomposite characterization*

The morphology of ACTF/Chitosan was observed on scanning electron microscopy (SEM) (Carl Zeiss, Germany). Fourier Transform Infrared Spectroscopy (FTIR) analysis using Shimadzu 6100A spectrometer. The spectral range is 400-4000 cm<sup>-1</sup>. Data of X-ray diffraction (XRD) were obtained by (Bruker AXS, Germany) (Cu Kα1 radiation, λ=1.54059 Å). In addition, Raman microscope model (SENTERRA, Bruker, Germany) was also used to characterize ACTF, at a laser wavelength of 532 nm and power 10 mW.

#### *Adsorption modeling and optimization*

##### *Effect of solution pH*

Effect of pH on adsorption capacity of Ca<sup>2+</sup> and Ba<sup>2+</sup> onto Chitosan /ACTF was evaluated. Batch

experiments were performed at pH from 2 to 7 using an adsorbent dose of 1 g/l and ion solutions volume 50 ml at room temperature for 24 h, where the initial concentration of Ca<sup>2+</sup> and Ba<sup>2+</sup> were 100 mg/l. The pH of the initial solution was adjusted by using 0.1 M HCl and 0.1 M NaOH.

##### *Effect of contact time*

Contact time effect was evaluated by a constant mass (1 g/l) of Chitosan /ACTF with a fixed volume (50 ml) of four concentrations (25, 50, 75 and 100 mg/l) for different intervals of contact time until equilibrium was reached.

##### *Effect of biocomposite treatment dose*

The effect of changing biocomposite dosage on the removal of calcium and barium ions was examined at different values changing from 0.05 g/l to 0.75 g/l. The optimum pH was then and adsorption tests were done at pH 6 and equilibrated for 24 hours.

##### *Adsorption studies*

The batch mode was applied for the sorption studies. An amount of 0.5 g of Chitosan/ACTF beads was added into 50 mL of different initial concentrations of Ca<sup>2+</sup> and Ba<sup>2+</sup> solutions. The experiments were done at different temperatures (25°, 45°, 65°, and 75°C) and pH 6. After shaking in isothermal water-bath shaker for 70 min at 250 rpm shaking rate until equilibrium was reached, contents were centrifuged. The Ca<sup>2+</sup> and Ba<sup>2+</sup> contents of the supernatants were determined by atomic absorption spectrophotometer for Ca<sup>2+</sup> and Ba<sup>2+</sup> respectively.

The quantity absorbed by a unit mass of an adsorbent at equilibrium (q<sub>e</sub>) and the adsorption percentage (%) at an instant was calculated using equation 1 and equation 2 respectively as follows:

$$q_e = \frac{(C_0 - C_e)V}{m} \quad (1)$$

$$q_e = \frac{(C_0 - C_e)V}{m} \times 100 = \frac{(C_0 - C_e)}{C_0} 100 \quad (2)$$

Where C<sub>0</sub> and C<sub>e</sub> are the initial and equilibrium concentrations of adsorbate solution (mg/l), respectively. V is the total volume of the solution (l), and m is the mass of chitosan/ACTF used (g). The adsorption equilibrium data were fitted into three different isotherm models to determine the most suitable model to represent the adsorption process. Langmuir, Freundlich, and D-R isotherms. Kinetics and thermodynamics parameters were evaluated by varying contact time and concentrations (mg/l) at the optimum pH and adsorbent dose.

## Results and Discussion

### Characterization of Chitosan and Chitosan / ACTF Biocomposite

#### FTIR

In the FTIR spectrum of chitosan Fig. 1, the important characteristic bands at 3358, 2927, 1650 and 1591  $\text{cm}^{-1}$  were assigned to the overlapping of the N–H and O–H stretching vibration,  $-\text{CH}_2$  stretching mode,  $-\text{N}-\text{H}$  bending mode and C–O–C stretching vibration of chitosan. An intercalated structure for the chitosan/ACTF was achieved with the grafting and exfoliated as having a wrinkled structure due to the functionalization effect which had sharp edges structure that obtained at a high grafting ratio of chitosan with ACTF. It can be concluded that ACTF, with OH-, O-, and  $-\text{COOH}$  functional groups at the edges of the graphene layer of ACTF, is disperse within polar polymer matrices as a result of the interactions between the oxygen functional groups on the ACTF and the polar polymer backbone chains as showed for the peak at 1639 that corresponding to amide bond of chitosan amine with carboxylic group of ACTF. Besides oxygen, functional groups play an important role in water hydrogen bond formation with the synthesized biocomposite.

#### XRD

Figure 2 represents the XRD patterns of chitosan, ACTF and Chitosan/ACTF biocomposite as 2a, 2b, and 2c respectively. As shown in Fig. 2b, the ACTF sheets exhibited a peak at  $ca. 2\theta = 27^\circ$ , corresponding to the (002) crystallographic plane. This peak was observed in the case of the Chitosan/ACTF biocomposite (Fig. 2c) with a small deviation to  $28^\circ$  that show there are high chemical interaction between ACTF and chitosan chain. This implies that the oxygen functional groups were detached from the ACTF surface and the layers of ACTF are not aggregating with each other that causes amorphization in the crystalline structure of carbon nonmaterial's. In addition, the peak intensity of ACTF (at  $27^\circ$ ) decreased significantly, which means that the film crystallinity released after the biocomposite formation. Typical diffraction peaks of Chitosan were detected between  $12^\circ$  and  $21^\circ$ , similar to the previous works nanoparticle [20] [21]. The crystalline structure of chitosan and Chitosan/ACTF looks similar, showing sharper ACTF peaks at  $29^\circ$  and  $31^\circ$ . It implies the good crystallization of the polymer in the biocomposite, which due to the good dispersion of ACTF in the matrix and enhanced by the restriction of chitosan chains.

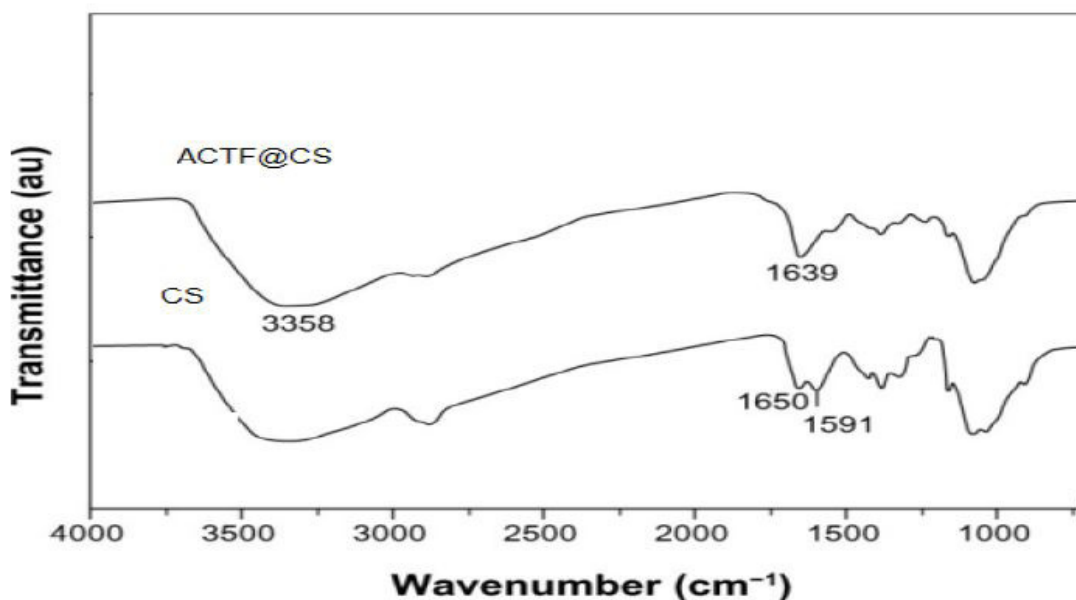


Fig. 1. FTIR of Chitosan and Chitosan/ACTF biocomposite

### SEM

SEM image (Fig. 3a) exhibits the morphology of chitosan flakes subjected to modification by microwave irradiation. It is clear to observe chitosan surface with the spherical cavities in addition to a large number of opened cells in a spongy structure. After the deposition process of Chitosan/ACTF biocomposite (Fig.3b), the surface morphology has changed dramatically, which confirms that the thick Chitosan/ACTF biocomposite had been successfully deposited. The cavitation porous skeleton structure clearly refers to the excellent crosslinking effect of the novel ACTF onto chitosan and indicates the unique folded morphology of adjacent cavities with an organized network of opened and semi-closed pores, which serves as an electron current collector and provides a large surface area.

In addition, folded chitosan sheets on ACTF; which appear as a sandwich-like structure (in some positions); indicate to the compatibility of ACTF and chitosan. Presence of these nodes works clearly to prevent chitosan sheets agglomeration and restocking with each other. The heterogeneous structure of the surface of the synthesized biocomposite makes full use of the surface area of ACTF, resulting in different readily accessible active sites for ion exchange and adsorption with coordination activity for the chitosan polymer chains with high electron density on internal and external surfaces which leads to highly effective metal affinity.

### Raman

Raman is a valuable spectroscopic technique Fig.4. shows the Raman spectra of the chitosan. The prominent Raman peaks can be assigned by sharp peak at (1310-1350  $\text{cm}^{-1}$  and 1440-1490  $\text{cm}^{-1}$ ) exhibit amide. The C-C stretching region appears at (1050-1200  $\text{cm}^{-1}$ ), the C-NH bending region appears at (1290-1350  $\text{cm}^{-1}$ ).

Raman spectroscopic technique for identifying the carbon materials, especially the  $\text{sp}^2$  and  $\text{sp}^3$  hybridized carbon atoms in chitosan/ACTF biocomposite, the results are displayed in Fig. 5. The D band is an indication of the disorder vibrations and defects of the  $\text{sp}^3$  carbon atoms, and the G band is related to the vibration of  $\text{sp}^2$  carbon atoms in a graphitic 2D hexagonal lattice. But the G bands of the chitosan/ACTF biocomposite appeared 1534  $\text{cm}^{-1}$  blue-shifted in comparison with that of the ACTF and the D band appear at 1391  $\text{cm}^{-1}$  with intensity value

near the value of G band and that indicator for the presence of activated carbon body in between the graphene sheets that form ACTF structures. The results indicate that the ACTF/biocomposite contains ACTF sheets can influence the graphene sheets (the existence of electronic interaction between ACTF sheets and chitosan) in the ACTF carbon nanostructure. The intensities of the D and G bands ( $I_D$ ,  $I_G$ ) provide evidence to the ordered or disordered crystalline structures of ACTF sheets. The presence of wide broadband at 3000  $\text{cm}^{-1}$ , refers to the presence of separate graphene sheets, which put a light spot on the form cross-liked ACTF in the biocomposite. Chitosan sheets may be embedded into the crystalline structure of ACTF, and this emphasizes the change in the crystalline form of the two components.

### Adsorption modeling and optimization

#### Effect of pH

Metal ion solution pH is one of the most significant parameters in the adsorption process because it affects the solubility of the metal ions, degree of ionization, the functional groups of the adsorbent. In order to examine the effects of initial solution pH on the uptake of  $\text{Ca}^{2+}$  or  $\text{Ba}^{2+}$ , sorption experiments were conducted at different pH values ranging between 2 and 7 and the results were illustrated in Fig. 6. In order to avoid the precipitation,  $\text{pH} > 7.0$  were ignored. The adsorption capacity of Chitosan/ACTF for  $\text{Ca}^{2+}$  or  $\text{Ba}^{2+}$  was small at low pH values. The results for both  $\text{Ca}^{2+}$  and  $\text{Ba}^{2+}$  uptake showed that the removal efficiency increases with pH increasing from 2 to a maximum value at pH 6 and 6.5 respectively; where the maximum removal efficiency was (96.3%) for  $\text{Ca}^{2+}$  and by increasing pH up to 7 the removal efficiency slightly decreased. On the other hand, the maximum efficiency for  $\text{Ba}^{2+}$  was (97.1%) at pH 6.5 with no notable further change.

It is known that the functional groups such as amino groups ( $-\text{NH}_2$ ) and hydroxyl groups ( $-\text{OH}$ ) are included in chitosan, and in strongly acidic solutions, more protons will be available to protonate amino groups of chitosan to form  $-\text{NH}_3^+$  group, which leads to reducing the number of adsorption binding sites [21].

On the other side, a previous study of pH effect on adsorption capacity of ACTF for  $\text{Na}^+$  referred to the same behavior at pH ranging from 1 to 11 [11]. Hence, in the present work, a pH of a value of 6 was selected as the optimum for further experimental work.

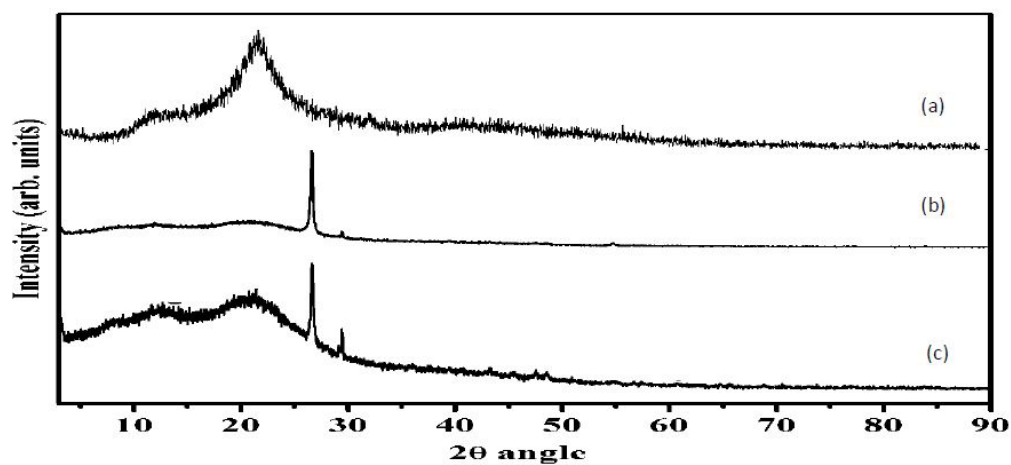


Fig. 2. XRD patterns of (a) Chitosan, (b) ACTF, (c) Chitosan/ACTF biocomposite.

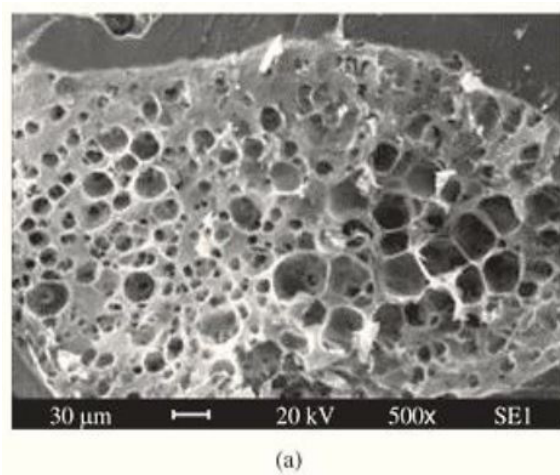


Fig. 3a. SEM images of Chitosan

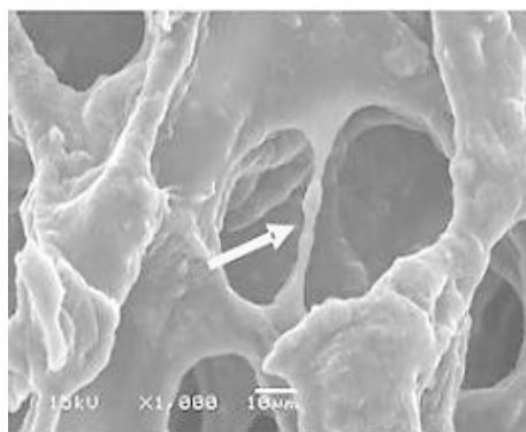


Fig 3b. SEM images of Chitosan/ACTF biocomposite

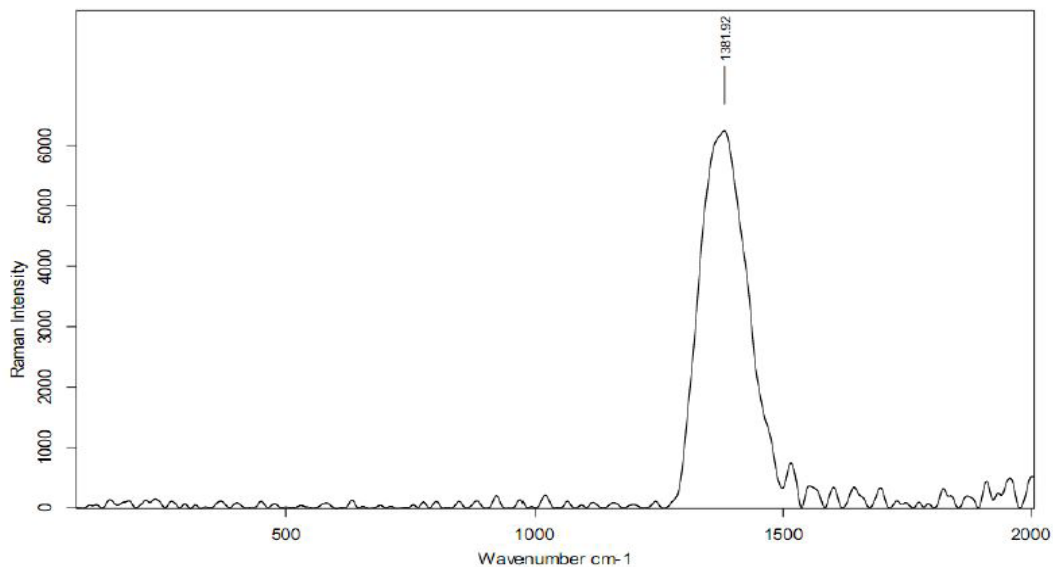


Fig. 4. Raman analysis for extracted chitosan

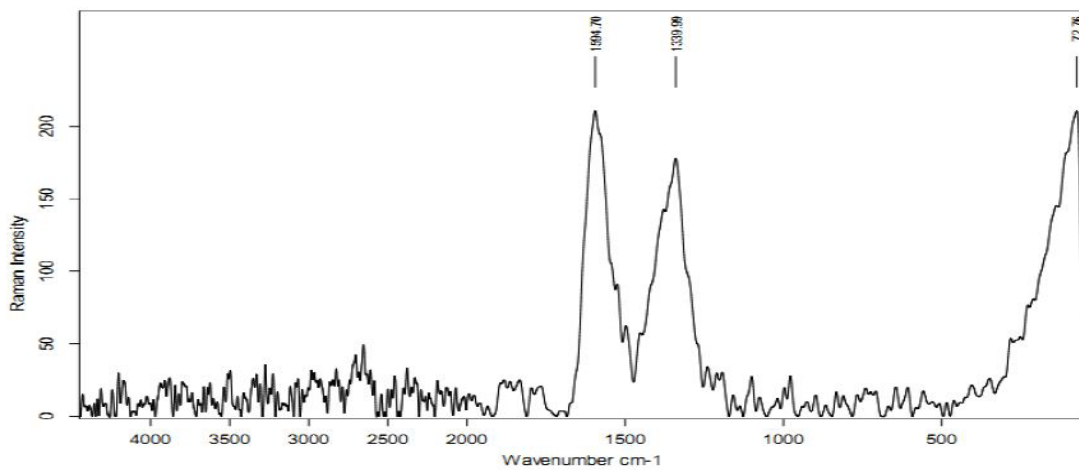


Fig. 5. Raman analysis of Chitosan/ACTF biocomposite

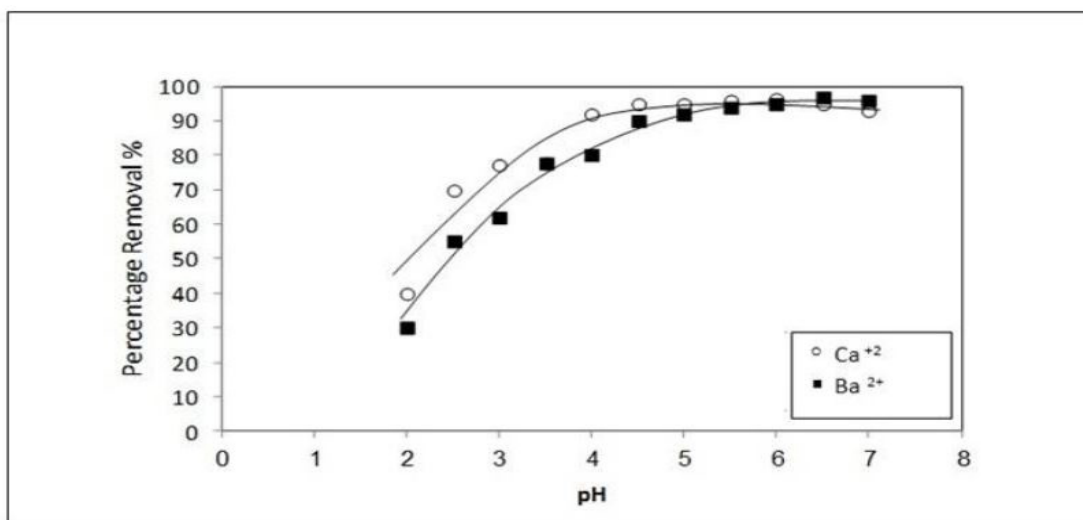


Fig. 6. Effect of pH on the removal efficiency of Ca<sup>2+</sup> and Ba<sup>2+</sup> onto Chitosan/ACTF biocomposite

#### *Effect of contact time*

The adsorption versus time of  $\text{Ca}^{2+}$  and  $\text{Ba}^{2+}$  onto Chitosan/ACTF biocomposite at four different initial concentrations, 10, 25, 50 and 100 mg/l at 25°C and pH 6 was illustrated in (Figs.7&8). It is obvious from experimental data that, the removal efficiency % increases with time and attains equilibrium in 65 min for concentrations 10, 25 and 50 mg/l, but it takes about 70 min to reach equilibrium for 100 mg/l. The removal of  $\text{Ca}^{2+}$  and  $\text{Ba}^{2+}$  onto Chitosan/ACTF biocomposite was fast in the initial stages and gradually decreases by time until saturation and the removal efficiency % was reached 80 % and 87.85 % for  $\text{Ca}^{2+}$  and  $\text{Ba}^{2+}$  respectively, where initial concentration was 100 mg/l thus, 70 min was the optimal contact time for the rest the experimental study.

#### *Effect of adsorbent dose*

Under the optimized conditions of pH (6.5) and contact time (70 min), sorption behavior of Chitosan/ACTF at different dosages from 0.05 g/l to 0.75g/l, have been studied in 100 mg/l of  $\text{Ca}^{2+}$  and  $\text{Ba}^{2+}$  solutions. The maximum removal of  $\text{Ca}^{2+}$  and  $\text{Ba}^{2+}$  cations was 89.9% and 70% respectively with 0.75 g/l dosage of the biocomposite (Fig. 9). The observed behavior can be divided into two stages. In the first stage (0.05 g/l to 0.5 g/l), similar adsorption capacity is remarkable for both cations. But a different response to further increase in adsorbent dosage appears in the second stage (0.5 g/l to 0.75 g/l. Therefore, 0.5 g/l was considered as the optimal adsorbent dose for the rest of the study. The increase in adsorption percentage with increasing adsorbent dose arises because of the increased availability of surface area or exchange sites at higher concentrations of adsorbents.

#### *Isotherm modeling*

The adsorption isotherm was established and compared by different three adsorption isotherms, namely Langmuir, Freundlich, and D-R models at different temperature (25°, 45°, 65°, and 75°C), under the optimized condition of pH, contact time and the adsorbent dose.

#### *Langmuir isotherm model*

Langmuir isotherm confirms the monolayer adsorption occurring on a homogenous adsorbent surface with no lateral interaction. The Langmuir expression may be converted into a linear form:

$$\frac{C_e}{q_e} = \frac{C_e}{q_{\max}} + \frac{1}{K_L q_{\max}} \quad (3)$$

*Egypt.J.Chem.* Vol. 62, Special Issue (Part 2) (2019)

Where,  $C_e$  is the concentration of metal ion in a batch system at equilibrium (mg/l),  $q_e$  is the amount of adsorption of  $\text{Ca}^{2+}$  and  $\text{Ba}^{2+}$  at equilibrium (mg/g),  $q_{\max}$  is the maximum adsorption capacity on the surface of chitosan (mg/g), and  $K_L$  is the equilibrium adsorption constant (l/g). A plot of  $C_e/q_e$  versus  $C_e$  gives a straight line with a slope of  $1/q_{\max}$ , and intercept is  $1/(K_L)$ .

The essential characteristics of the Langmuir isotherm can be expressed in terms of a dimensionless equilibrium parameter ( $R_L$ ):

$$R_L = \frac{1}{1 + a_L \cdot C_0} \quad (4)$$

Where  $R_L$  is a dimensionless constant separation factor, and  $a_L$  is the Langmuir adsorption constant (L/g.).

#### *Freundlich isotherm model*

The equilibrium data have been analyzed using the Freundlich isotherm as given by linear equation (5).

$$\log q_e = \log K_F + (1/n) \log C_e \quad (5)$$

Where  $n$  and  $K_F$  are the Freundlich constants.  $K_F$  and  $n$  are the Freundlich constants. The  $K_F$  value is related to the adsorption capacity; while  $1/n$  gives an indication of the favorability or adsorption and capacity of the adsorbent/adsorbate system. Values of ( $n$ ) greater than 1 represent favorable adsorption according to nanoparticle [20].

#### *Dubinin-Radushkevich (D-R) isotherm model*

This model is widely used for the description of adsorption in microporous materials, especially those of a carbonaceous origin. The equation is given as [23].

$$q_e = q_s \exp(-k_{ad} \epsilon^2) \quad (6)$$

$$\ln(q_e) = \ln(q_s) - (k_{ad} \epsilon^2) \quad (7)$$

Where  $q_e$ ,  $q_s$ ,  $K_{ad}$ , are  $q_e$  = amount of adsorbate on the adsorbent at equilibrium(mg/g);  $q_s$  = theoretical isotherm saturation capacity (mg/g);  $K_{ad}$  = Dubinin–Radushkevich isotherm constant ( $\text{mol}^2/\text{kJ}^2$ ) and Dubinin–Radushkevich isotherm constant. This approach was usually applied to distinguish the physical and chemical adsorption of metal ions with its mean free energy,  $E$  per molecule of adsorbate, which is the energy needed for removing a molecule from its location in the sorption space to the infinity. It is calculated as follows [24]:

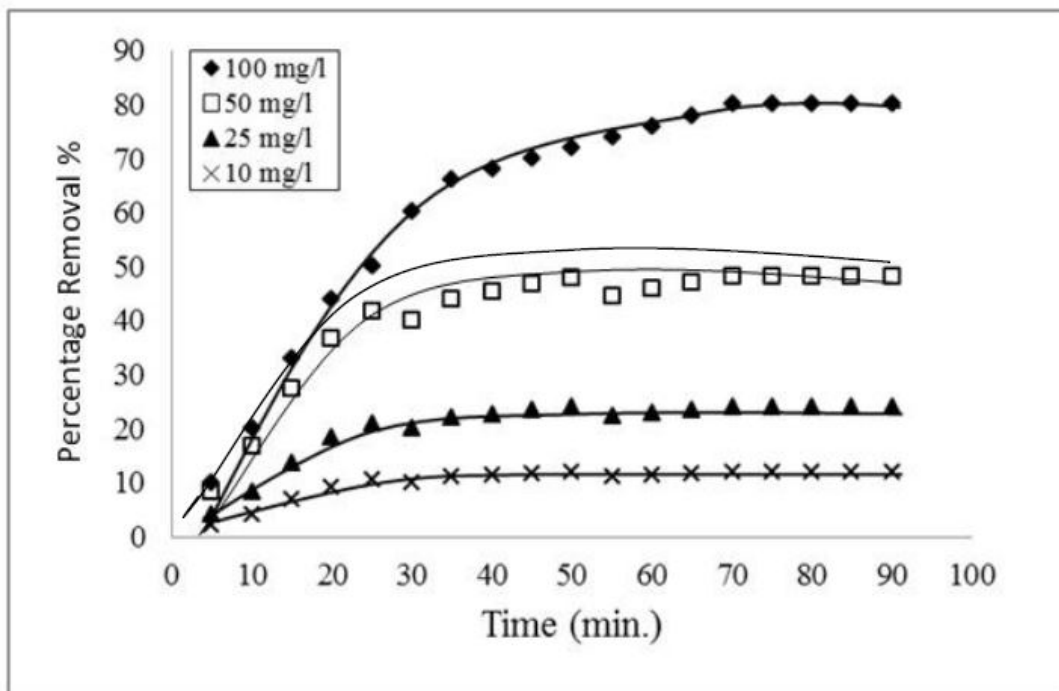


Fig. 7. Equilibrium Contact Time for the Adsorption of Ca<sup>2+</sup> onto Chitosan/ACTF biocomposite at Different Initial Concentrations

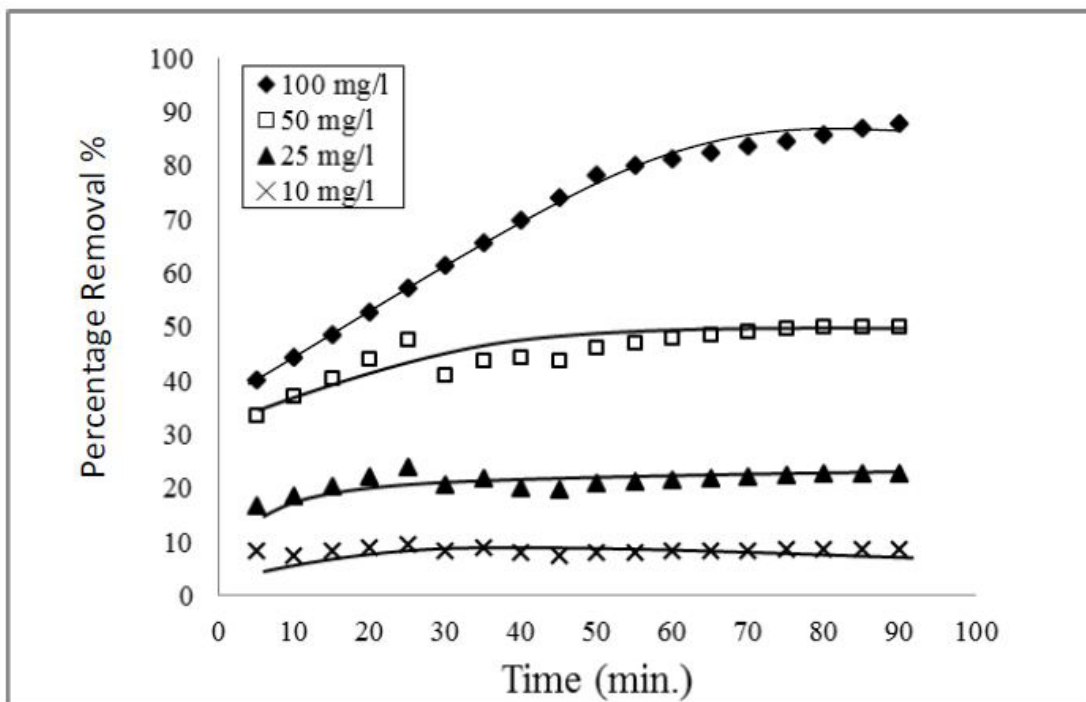


Fig. 8. Equilibrium Contact Time for the Adsorption of Ba<sup>2+</sup> onto Chitosan/ACTF biocomposite at Different Initial Concentrations

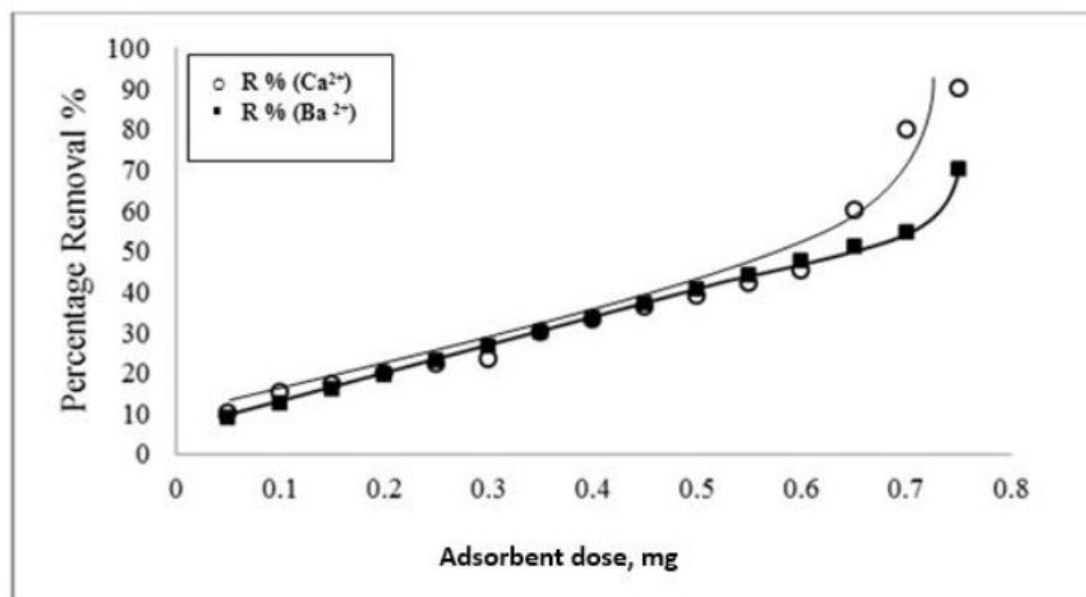


Fig. 9. Effect of adsorbent dose on the adsorption capacity of  $\text{Ca}^{2+}$  and  $\text{Ba}^{2+}$  onto Chitosan/ACTF biocomposite at Temp. =25 °C.

$$E = \frac{1}{\sqrt{2K_{ad}}} E = \frac{1}{\sqrt{2K_{ad}}} \quad (8)$$

Fig. 10 and 11 show the linearization plots of the applied isotherm models for  $\text{Ca}^{2+}$  and  $\text{Ba}^{2+}$ . The isotherm models parameters obtained for adsorption of at different temperatures are listed in Table 1. Equilibrium adsorption data fitted well to Freundlich. In this work, the values of  $n$  are greater than one which indicating favorable adsorption by Chitosan/ACTF biocomposite [25].

#### Kinetic studies

In order to determine the mechanism of the adsorption process, kinetic models have been proposed to give useful data to improve adsorption efficiency [5]. In the current study, the adsorption process mechanism was investigated by fitting pseudo-first-order and second-order reactions to the experimental data. The pseudo-first-order model is given by the Eq. (9):

$$\log(q_e - q_t) = \log q_{e,L} - \frac{K_L}{2.303} t \quad (9)$$

where,  $q_e$  and  $q_t$  are the adsorption capacities of Ca or Ba using chitosan at equilibrium and time  $t$ , respectively ( $\text{mol}\cdot\text{g}^{-1}$ ), and  $k_1$  is the rate constant of the pseudo-first-order adsorption ( $\text{h}^{-1}$ ). The linear form of the pseudo-second-order rate equation is given as follows:

$$\frac{t}{q_t} = \frac{1}{q_2^2 k_2} + \frac{t}{q_2} \quad (10)$$

where,  $q_e$  and  $q_t$  are the adsorption capacities of Ca or Ba using chitosan at equilibrium and time  $t$ , respectively ( $\text{mol}\cdot\text{g}^{-1}$ ), and  $k$  is the rate constant of the pseudo-second-order adsorption ( $\text{g}\cdot\text{mol}^{-1}\cdot\text{h}^{-1}$ ).

Tables 2 & 3 and Fig. 12-15 shows the values of the parameters of kinetic models. The results showed that the adsorption kinetics of  $\text{Ca}^{2+}$  and  $\text{Ba}^{2+}$  could be well described by the pseudo-second-order model. According to the  $R^2$  values, the pseudo-second-order model had the best fitting with the obtained data, which means that the concentrations of both the adsorbent and the adsorbate were the rate-controlling step ion adsorption onto the chitosan/ACTF. This also indicates that chemisorption is the dominant mechanism in the adsorption process, which involves the exchange or sharing of electrons between  $\text{Ca}^{2+}$  and  $\text{Ba}^{2+}$  and the binding sites on the ACTF/chitosan particles. It was reported that the chemisorption process that is confined to one layer of molecules on the surface of the adsorbent material, is usually followed by physically adsorbed layers of the adsorbate.

### Thermodynamics study

The thermodynamic parameters for adsorption of  $\text{Ca}^{2+}$  and  $\text{Ba}^{2+}$  on chitosan/ACTF were evaluated at different four temperatures (298, 308, 323 and 343 K) at the optimum solution pH and adsorbent dose. Results in Table 4 show the thermodynamic parameters: standard Gibbs free energy ( $\Delta G$ ), standard enthalpy ( $\Delta H$ ) and standard entropy ( $\Delta S$ ). The Gibbs free energy change of adsorption is defined as:

$$\Delta G^\circ = -RT \ln K_L \quad (11)$$

Where ( $K_L$ ) is Langmuir equilibrium constant, ( $R$ ) is the universal gas constant ( $8.314 \text{ J.g-mol}^{-1}.\text{K}^{-1}$ ) and ( $T$ ) is the absolute temperature (K). The values of ( $\Delta H$ ) and ( $\Delta S$ ) was computed using Van't Hoff equation nanoparticle [26]:

$$\ln K_L = \frac{\Delta S^\circ}{R} - \frac{\Delta H^\circ}{RT} \quad (12)$$

A plot of ( $\ln K_L$ ) versus ( $1/T$ ) (Fig. 16) should produce straight line with slope equals to  $-\Delta H/RT$  and intercept equals to  $\Delta S/R$ . The calculated values of ( $\Delta H$ ) and ( $\Delta S$ ) and ( $\Delta G$ ) are listed in Table 4

The standard enthalpy ( $\Delta H$ ) and entropy ( $\Delta S$ ) changes of adsorption determined from equation (12) were found to be  $-216.19 \text{ (kJ.mol}^{-1}\text{)}$  and  $32.779 \text{ (J. mol}^{-1}.\text{K}^{-1}\text{)}$ , respectively for  $\text{Ca}^{2+}$  and  $-143.99$  and  $30.82831 \text{ (kJ.mol}^{-1}\text{)}$  for  $\text{Ba}^{2+}$  ions. The magnitude of ( $\Delta H$ ) for physical adsorption ranges from 4 to 40 ( $\text{kJ.g-mol}^{-1}$ ), compared to that of chemical adsorption ranging from 40 to 800 ( $\text{kJ.g-mol}^{-1}$ ) nanoparticle [27]. The negative value of enthalpy ( $\Delta H$ ) distinguish the exothermic adsorption process, on the other hand the negative values of Gibbs free energy ( $\Delta G$ ) is an indicator for spontaneous behavior of the adsorption process with increasing in the negative value showing the more and more increasing in that with increasing temperature values in the two-state of metal ions under study .

The positive value of  $\Delta S$ , which indicates the increase in the molecules disorders during the adsorption process, which is due to the binding of the molecules with the adsorbent surface [28].

### Conclusions

- (1) From the above results and discussion, it became evident that the Chitosan/ACTF biocomposite copolymer was prepared successfully. The FTIR, TGA, XRD, and SEM, Raman results confirm the formation of biocomposite.
- (2) Chitosan/ACTF biocomposite exhibited high adsorption capacity for  $\text{Ca}^{2+}$  and  $\text{Ba}^{2+}$  under the optimal experimental conditions. The equilibrium is practically achieved in 70 min at optimum pH=6. The adsorption was found to increase with increased concentration and contact time while it decreased with increased temperature.
- (3) Thermodynamic parameters indicate an exothermic adsorption process.
- (4) Adsorption parameters for the Langmuir, Freundlich and D-R isotherms were determined.  $\text{Ca}^{2+}$  and  $\text{Ba}^{2+}$  adsorption on the Chitosan/ACTF biocomposite confirms to the move after the Freundlich adsorption model; suggest that the mechanism includes both chemisorptions and physisorption.
- (5) The pseudo-second-order kinetic model gives the mechanism and parameters suggesting that the rate-limiting step of the adsorption was a chemical process rather than a physical process like diffusion.
- (6) The experimental study suggests using Chitosan/ACTF biocomposite for the removal of divalent cations like calcium and barium ions in the groundwater.

**TABLE 1. Estimated Langmuir, Freundlich and D-R isotherm models parameters for adsorption of Ca<sup>2+</sup> and Ba<sup>2+</sup> onto Chitosan/ACTF biocomposite at different temperatures.**

Isotherm Model	Parameters	Temp.(°C)							
		25		45		65		75	
		Ca <sup>2+</sup>	Ba <sup>2+</sup>	Ca <sup>2+</sup>	Ba <sup>2+</sup>	Ca <sup>2+</sup>	Ba <sup>2+</sup>	Ca <sup>2+</sup>	Ba <sup>2+</sup>
Langmuir	$K (L mg^{-1})$	0.0113	0.0130	0.0109	0.01291	0.0083	0.00464	0.0068	0.005
	$q_0 (mg g^{-1})$	0.0222	0.4576	0.0122	3.4689	0.0109	2.004111	0.00021	1.5856
	$R_L$	0.92	0.4336	0.841	0.6832	0.881	0.6832	0.234	0.6844
	$R^2$	0.9991	0.7725	0.9995	0.9571	1.000	0.9612	0.7412	0.8552
Freundlich	$K_f$	0.5122	1.6552	0.4706	0.1839	0.7904	0.38327	0.96929	0.0126
	$n$	1.2907	1.8531	1.4290	1.6388	1.2276	2.8621	0.22101	1.7828
	$R^2$	0.7936	0.999	0.8058	0.9986	0.9262	0.8952	0.9965	0.9836
D-R	$qm (mol g^{-1})$	4.4061	4.1844	4.5761	4.9489	4.21761	4.97869	5.36462	4.1814
	$K (mol^2 kJ^{-2})$	$4.76 \times 10^{-7}$	0.0005	4.5761	$5.1 \times 10^{-5}$	$2.5 \times 10^{-7}$	0.00146	$8.7 \times 10^{-7}$	$6 \times 10^{-5}$
	$E (kJ mol^{-1})$	10.024	31.255	13.280	98.860	14.195	18.447	20.258	91.083
	$R^2$	0.8834	0.9998	0.9872	0.9661	0.9433	0.9908	1.000	0.9467

**TABLE 2. kinetics Constants for the Adsorption of Ca<sup>2+</sup> onto Chitosan/ACTF**

kinetics model	Variables			
	$C_0$ (mg./l)	$k_1$ (min <sup>-1</sup> )	$q_1$ (mg.g <sup>-1</sup> )	$R^2_1$
First-order	100	-0.00791	0.277433	0.95615
	50	-0.01575	0.166248	0.92754
	25	-0.01575	0.066459	0.92754
	10	-0.00951	0.16601	0.89914
Second-order	$C_0$ (mg./l)	$k_2$ (g.mg <sup>-1</sup> .min <sup>-1</sup> )	$q_2$ (mg.g <sup>-1</sup> )	$R^2_2$
	100	60.22883	0.016603	0.981515
	50	10.47201	0.095493	0.99347
	25	50	0.02	1.0
	10	10	0.1	1.0

**TABLE 3. kinetics Constants for the Adsorption of Ba<sup>2+</sup> onto Chitosan/ACTF**

kinetics model	Variables			
	$C_0$ (mg./l)	$k_1$ (min <sup>-1</sup> )	$q_1$ (mg.g <sup>-1</sup> )	$R^2_1$
First-order	100	-0.00791	0.277433	0.95615
	50	-0.01575	0.166248	0.92754
	25	-0.01575	0.066459	0.92754
	10	-0.00951	0.16601	0.89914
Second-order	$C_0$ (mg./l)	$k_2$ (g.mg <sup>-1</sup> .min <sup>-1</sup> )	$q_2$ (mg.g <sup>-1</sup> )	$R^2_2$
	100	52.51158	0.019043	0.998031
	50	10.47201	0.095493	0.99347
	25	50	0.02	1
	10	10	0.1	1

**TABLE 4. Thermodynamic parameters of Ca<sup>2+</sup> and Ba<sup>2+</sup> adsorption onto Chitosan/ACTF biocomposite**

Adsorbate	Temp. (K)	$\Delta G$ KJ.mol <sup>-1</sup>	$\Delta H$ kJ.mol <sup>-1</sup>	$\Delta S$ J.mol <sup>-1</sup> .K <sup>-1</sup>
Ca <sup>2+</sup>	298	-31.387	-216.19	32.779
	308	-31.714		
	323	-32.206		
	343	-32.862		
Ba <sup>2+</sup>	298	-23895	-143.99	30.82831
	308	-24.357		
	323	-24974		
	343	-25590.5		

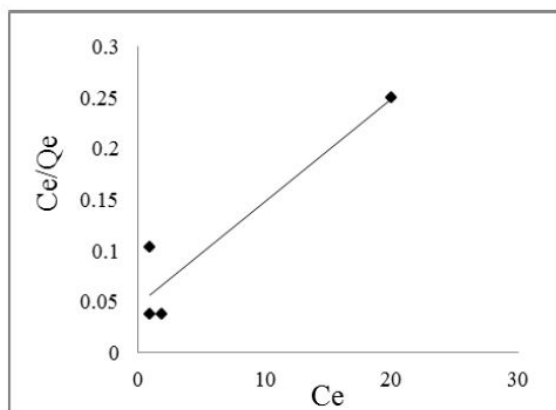


Fig. 10 (a). Langmuir plot for the adsorption of  $\text{Ca}^{+2}$  onto Chitosan/ACTF biocomposite

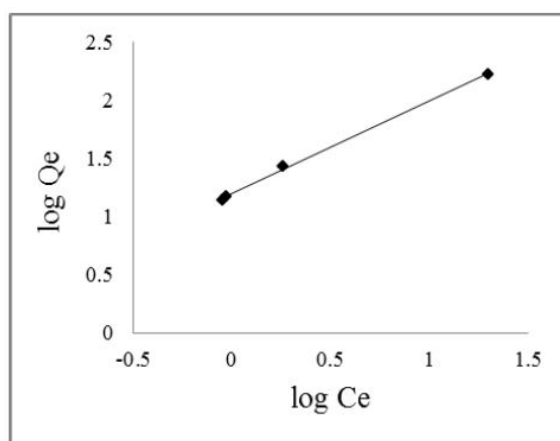


Fig. 10 (b). Freundlich plot for the adsorption of  $\text{Ca}^{+2}$  onto Chitosan/ACTF biocomposite

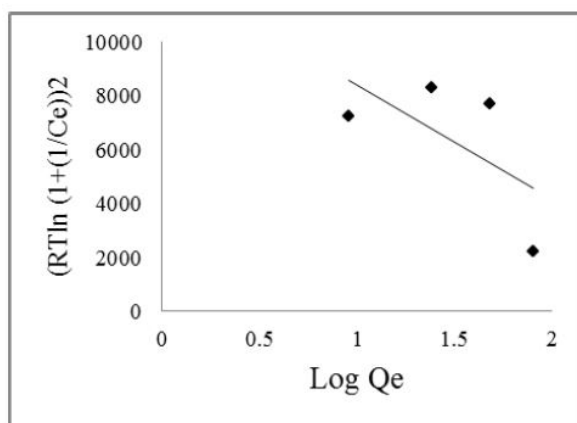


Fig. 10 (c).  $D-R$  plot for the adsorption of  $\text{Ca}^{+2}$  onto Chitosan/ACTF biocomposite

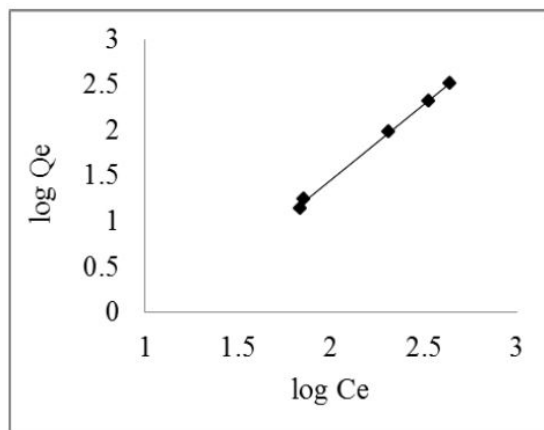


Fig. 11 (a). Langmuir plot for the adsorption of  $Ba^{+2}$  onto Chitosan/ACTF biocomposite

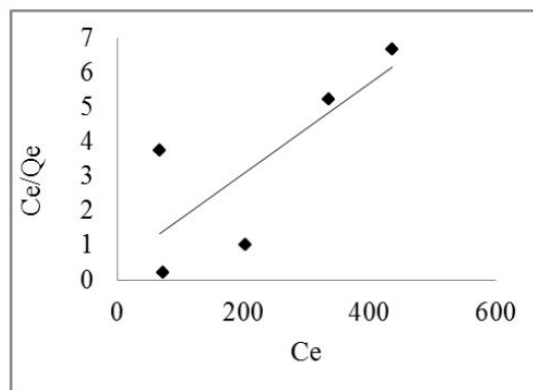


Fig. 11 (b). Freundlich plot for the adsorption of  $Ba^{+2}$  onto Chitosan/ACTF biocomposite

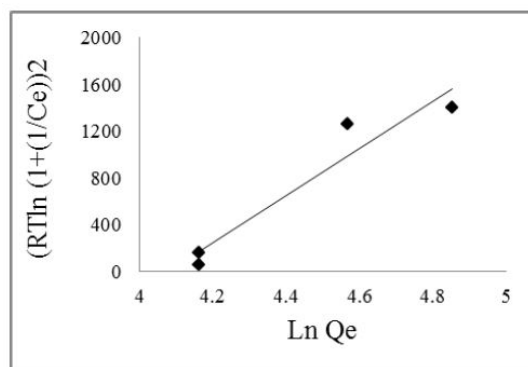


Fig. 11 (c).  $D-R$  plot for the adsorption of  $Ba^{+2}$  onto Chitosan/ACTF biocomposite

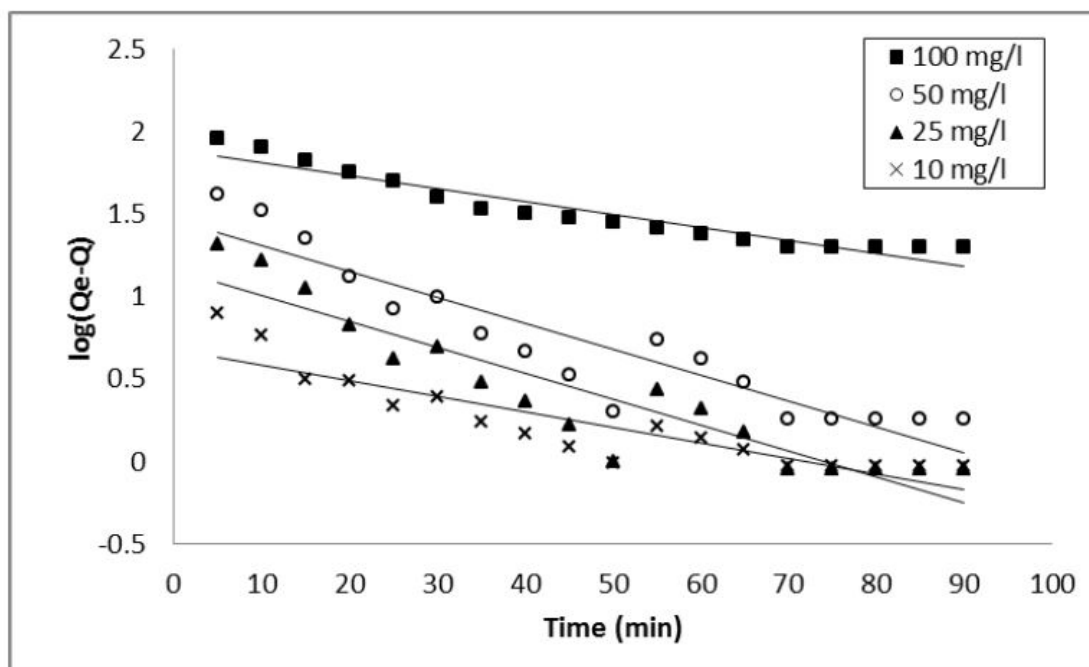


Fig. 12. Pseudo- First order kinetics model for the adsorption of  $\text{Ca}^{2+}$  onto Chitosan/ACTF biocomposite at different initial concentration

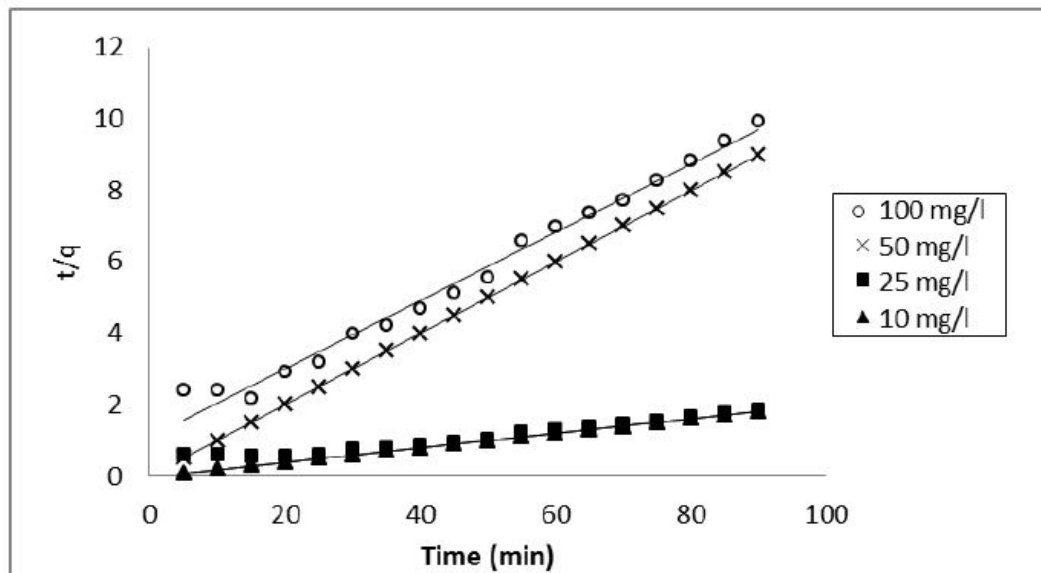


Fig. 13. Pseudo- Second-order kinetics model for the adsorption of  $\text{Ca}^{2+}$  onto Chitosan/ACTF biocomposite at the different initial concentration

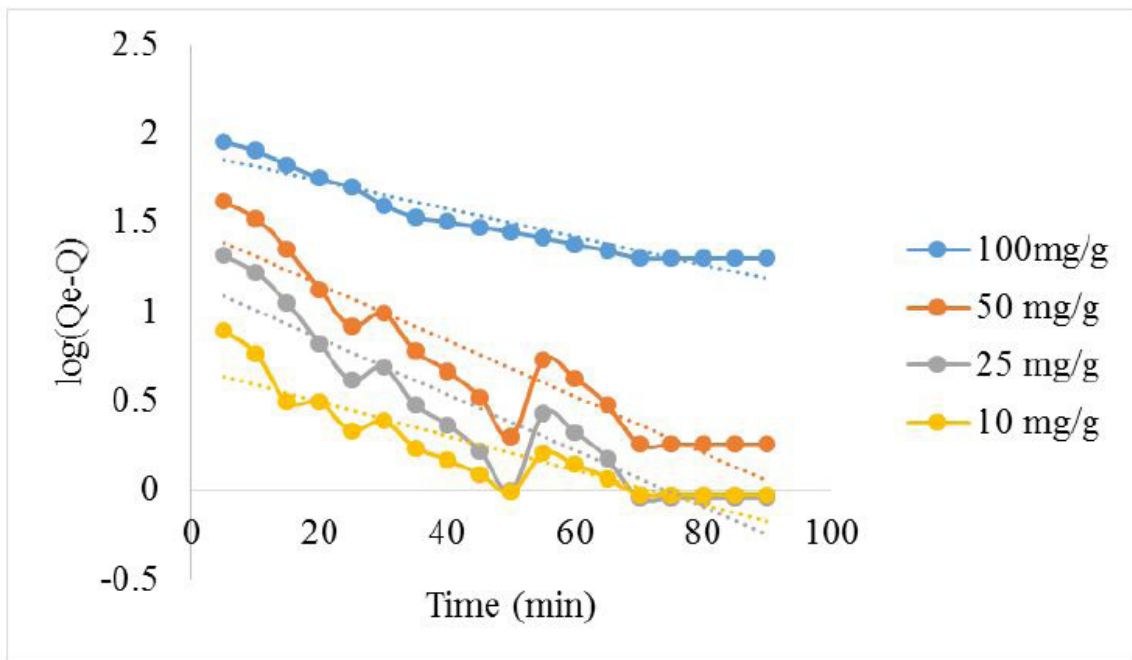


Fig. 14. Pseudo- First-order kinetics model for the adsorption of Ba<sup>2+</sup> onto Chitosan/ACTF composite at the different initial concentration

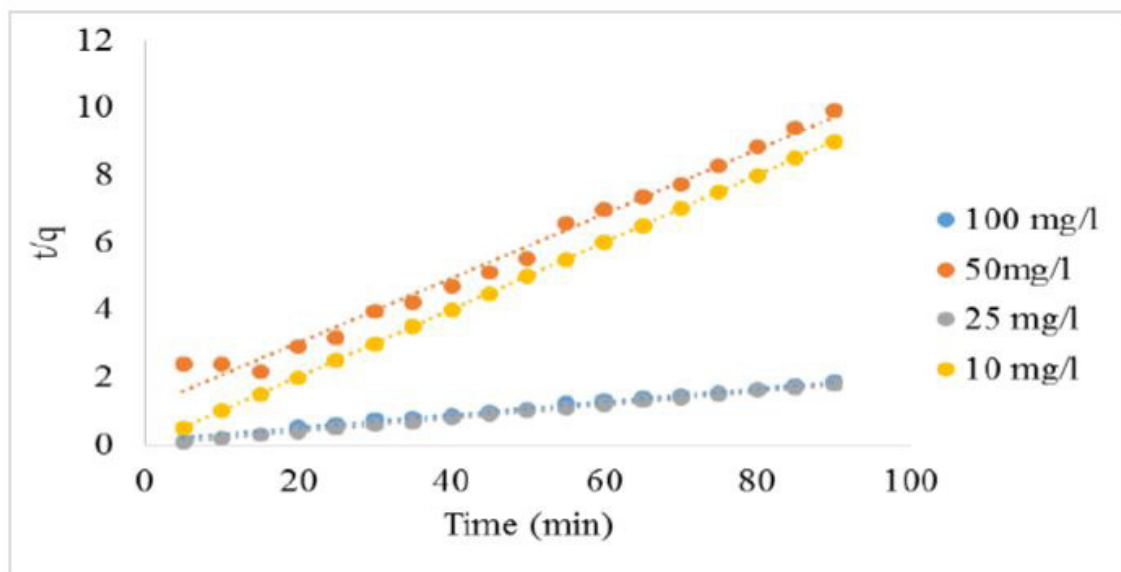


Fig. 15. Pseudo- Second-order kinetics model for the adsorption of Ba<sup>2+</sup> onto Chitosan/ACTF composite at a different initial concentration

## Acknowledgments

The authors gratefully acknowledge the financial support from Cairo University, Egyptian Petroleum Research Institute and Beni-Suef University.

## References

1. Menkiti M.C. and Onukwuli O.D., Impact of pH Variation on Coag-flocculation Behaviour of Chitin Derived Coag-flocculant in Coal Washery Effluent Medium. *Journal of Minerals & Materials Characterization & Engineering*. **10** (15), 1391-1407 (2011).
2. Pentamwa, P., Thiphara, W. and Nuangon, S., Hardness Removal from Groundwater by Synthetic Resin from Waste Plastics, *International Conference on Environmental and Computer Science* Singapore. IPCBEE, 19 IACSIT Press, Singapore (2011)
3. Zsófi, Z., Villangó, S., Pálfi, Z., Tóth, E. and Balo, B., Texture characteristics of the grape berry skin and seed (*Vitis vinifera* L. cv. Kékfrankos) under post veraison water deficit. *Sci. Hortic.* **172**, 176–182 (2014).
4. Cahyaningrum, S. E., Narsito, N., Santoso, S.J., and Agustini, R., Adsorption of Mg (II) ion from aqueous solution on chitosan beads and chitosan powder. *Journal of Coastal Development*. ISSN 1410-5217. **13** (3), 179-184 (2010).
5. Kano, N., Otsuki, Y., Lu, H. and Imaizumi, H., Study on Reduction of Chromium Using Humic Substances and Clay Minerals. *Journal of Ecotechnology Research*, **13**, 79-84 (2007).
6. Fathy M, Abdel Moghny, Th, Mousa, M.A, El-Bellihi, A.A-A and Awadallah A.E., Sulfonated Ion Exchange Polystyrene Biocomposite Resin for Calcium Hardness Removal. *International Journal of Emerging Technology and Advanced Engineering*. **5** (11), 20-29 (2015).
7. Mahatmanti F. W, Nuryono, N., and Narsito, N., Adsorption of Ca(II), Mg(II), Zn(II), and Cd(II) on Chitosan Membrane Blended with Rice Hull Ash Silica and Polyethylene Glycol. *Indones. J. Chem.*, **16** (1) 45- 52 (2016).
8. Mohseni-Bandpi, A., Kakavandi, B., Kalantary, R. R., Azarid, A. and Keramatid, A., Development of a novel magnetite–chitosan biocomposite for the removal of fluoride from drinking water: adsorption modeling and optimization. *RSC Adv.*, **5**, 73279–73289 (2015).
9. Ismail, A.F. and Yim, M.-S., Investigation of activated carbon adsorbent electrode for electrosorption-based uranium extraction from seawater. *Nucl. Eng. Technol.* **47** (5), 579–587(2015).
10. Bevilacqua, M., Babutskyi, A. and Chrysanthou, A. A review of the catalytic oxidation of carbon–carbon biocomposite aircraft brakes. *Carbon*. **95**, 861–869 (2015).
11. Fathy, M, Mousa, M.A., Abdel Moghny, T.H., El-Bellihi, A.A-A. and Awadallah, A.E., Novel Amorphous Carbon Thin Film (ACTF) from rice straw to remove sodium ions from synthetic saline water. *Adv. Recycl. Waste Manag.* 1–2 (2016).
12. Fathy, M., Abdel Moghny, Th., Mousa, M. A., El-Bellihi, A.A-A., Awadallah, A. E., Synthesis of Transparent Amorphous Carbon Thin Films from Cellulose Powder in Rice Straw. *Arab J Sci Eng.* **42**, 225–233 DOI 10.1007/s13369-016-2273-5 (2017).
13. El-Sayed, M. Ramzi, M., Hosny, R., Fathy, M., Abdel Moghny, Th., Breakthrough curves of oil adsorption on novel amorphous carbon thin film. *J. Water Sci. Technol.* **7** (3) 10, 2361–2369 (2016).
14. Fathy, M., Hosny, R., Keshawy, M. and Gaffer, A., Green synthesis of graphene oxide from oil palm leaves as novel adsorbent for removal of Cu(II) ions from synthetic wastewater, *Graphene Technology*, **4** (1-2), 33–40 June (2019)
15. Puligundla, P., Oh, S., and Mok, C., Microwave-assisted pretreatment technologies for the conversion of lignocellulosic biomass to sugars and ethanol: a review, *Carbon Letters*. **17** (1), 1-10 (2016).
16. Fathy M, El-Sayed, M., Ramzi, M. and Abdelraheem O.H., Adsorption separation of condensate oil from produced water using ACTF prepared of oil palm leaves by batch and fixed bed techniques, *Egyptian Journal of Petroleum*. **27** (3), 319–326 (2018).
17. Fu, W., Yang, H. S. Liu, Hari-Bala, Liu, S., Li, M. and Zou G., Preparation and characteristics of core– shell structure cobalt/silica nanoparticles. *Mater. Chem. Phys.* **100**, 246–250 (2006).
18. Hosny, R., Th. Abdel-Moghny, Ramzi, M.,

- Desouky, S. E. M. and Shama, S.A., Preparation and Characterization of Natural Polymer for Treatment of Oily Produced Water, *International Journal of Current Research*, **6** (3), 5413-5418 (2014).
19. Farrokhi-Rad M., Shahrabi T., Mahmoodi S., Khanmohammadi Sh., Electrophoretic deposition of hydroxyapatite-chitosan-CNTs nanocomposite coatings, *Ceramics International*, **43** (5), 4663-4669 (2017).
  20. Theophile, N. and Jeong, H. K., Electrochemical properties of poly(vinyl alcohol) and graphene oxide biocomposite for supercapacitor applications. *Chemical Physics Letters*, **669**, 125-129 (2017).
  21. Dong, Y., Yung, K.C., Ma, R., Yang, X., Chui, Y-S. and Lee, J-M., Zapfen, J.A., Graphene/acid assisted facile synthesis of structure-tuned Fe<sub>3</sub>O<sub>4</sub> and graphene biocomposites as anode materials for lithium ion batteries. *Carbon*. **86**, 310-317 (2015).
  22. Kousalya, G. N., Rajiv G. M. and Meenakshi, S., Sorption of Chromium (VI) Using Modified Forms of Chitosan Beads. *International Journal of Biological Macromolecules* .**47**, 308-315 (2013).
  23. Treybal, R. F. Mass Transfer Operation. Academic Press, New York. (1981).
  24. Dubinin, M.M. and Radushkevich, L.V., Equation of the Characteristic Curve of Activated Charcoal Proceedings of the Academy of Sciences. *Physical Chemistry Section USSR*, **55**, 331-333 (1947).
  25. Foo, K.Y. and Hameed B.H., Insights into the modeling of adsorption isotherm systems. *Chemical Engineering Journal*. **156**, 2-10 (2010).
  26. Amin, N. K., Removal of direct blue-106 dye from aqueous solution using new activated carbons developed from pomegranate peel: Adsorption equilibrium and kinetics. *Journal of Hazardous Materials*, **165** (1-3), 52- 62 (2009).
  27. Crini, G. and Badot, P., Application of chitosan, a natural aminopolysaccharide, for dye removal from aqueous solutions by adsorption processes using batch studies: A review of recent literature. *Prog. Polym. Sci.* **33**, 399-447 (2008).
  28. Gupta, V.K., Ali, I., Suhas and Mohan, D., Equilibrium uptake and sorption dynamics for the removal of a basic dye (basic-red) using low-cost adsorbents. *J. Colloid Int. Sci.* **265**. 257 -264 (2003).

في هذه الدراسة ، تم تحضير مركب حيوي مترابط له قدرة امتصاص عالية من خلال دمج غشاء كربوني رقيق غير متبلور (ACTF) ؛ تم تحضيره من قش الأرز بواسطة طريقة رش حمض الحفاز ؛ في مصفوفة البوليمرية الحيوية لثيتوزان بواسطة تقنية الترسيب بتشيع الميكروويف. تعمل التقنية الجديدة على تحسين تأثير الارتباط المتقاطع البوليمري بين ACTF والثيتوزان بدون محفز ولا تؤثر على التركيب الكيميائي للثيتوزان. تم تقييم الخواص الفيزيائية والكيميائية للمركب الناتج بواسطة FTIR و SEM و XRD و Raman وتشير تحاليل للثيتوزان/ ACTF إلى وجود مسام كهفية الشكل ، وكثافة عالية للإلكترون ومواقع نشطة لتبادل الأيونات على الأسطح الداخلية والخارجية بالإضافة إلى الثبات الحراري العالي. تلخص دراسة الامتزاز إمكانات متراكب الثيتوزان/ ACTF لإزالة ايونات الكالسيوم والباريوم من الماء عن طريق الامتزاز الدفعي. تم تجهيز أفضل نموذج حراري Freundlich ببيانات التوازن ، كما كان النموذج الحركي من الدرجة الثانية أفضل تركيب لبيانات الحركة الامتزازية. من خلال دراسات الديناميكي الحرارية ( $\Delta G$ ) و ( $\Delta H$   $\Delta S$ ) اتضح ان عملية الامتزاز لايونات الكالسيوم والباريوم طاردة للحرارة وان لها سعة امتزازية لهذه الايونات 80 ملليجرام/ جم و ٨٧,٨٥ ملليجرام/ جم بتركيز أولي ١٠٠ ملليجرام / لتر ، للكالسيوم وللباريوم على التوالي. واخيرا اشارت النتائج إلى ان متراكب الثيتوزان/ ACTF له قدرة امتزاز عالية وتوافقية ممتاز للمياه.